

Compensation for Temperature Dependency of 1D Position Sensitive Detector

Han Woong Yoo^a, David Brunner^a, Thomas Thurner^b, and Georg Schitter^a

^aTU Wien, Automation and Control Institute (ACIN), Gusshausstrasse 27-29, 1040 Vienna, Austria

^bInfinion Technologies Austria AG, Design Center Graz, Babenbergerstraße 10, 8020 Graz, Austria

ABSTRACT

PSDs are used for fast and precise beam position measurements in various applications such as scanner characterization and scanning probe microscopy. However, PSDs suffer from systematic position sensing errors at high temperatures, limiting the possible application fields for usage of PSDs. This paper investigates temperature dependency of PSDs and its compensation that enables the usability of PSDs in high temperature applications above 60 °C. The proposed compensation scheme is explained by the diode leakage current model, which is extended to the given semiconductor device structure of the PSD. For the validation of the proposed method, an experimental PSD characterization setup has been used, showing that the proposed temperature compensation scheme reduces the temperature-induced relative position sensing error from 44.7 % down to 0.2 % for temperatures up to 95 °C.

Keywords: Position sensitive detector (PSD), High temperature operation, Leakage current, Point drift measurement, Reliability test

1. INTRODUCTION

Position sensitive detector (PSD), also called position sensitive device, is a special type of photodiodes that measures the position of a light beam spot, estimating the center of gravity of the light distribution within the active area. There are two main types of PSD: segmented PSDs such as quadrant photodetectors and lateral effect PSDs.¹ In contrast to segmented PSDs, lateral effect PSDs have a large and linear position detection range regardless of shape and size of the beam spot. While active pixel sensors such as CCD and CMOS sensors can be used for the beam position detection with high linearity,² lateral effect PSDs are beneficial by seamless analog information of the beam spot position with low latency as well as high position resolution and a wide analog bandwidth due to its simple readout structure. From these benefits, PSDs are widely used in various applications such as a fast tracking control of micro medical robotics,³ displacement and vibration measurement of a motor shaft,⁴ scanning probe microscopy,⁵ atmospheric turbulence measurements,⁶ spectrometer,⁷ and evaluation of micro mirror deflection.^{8,9}

In some applications, for example a characterization of the temperature behavior of micro scanner devices for automotive lidar systems,⁹ PSDs are required to cope with various temperatures from -40 °C to 85 °C or even up to 125 °C.¹⁰ Low temperatures usually do not cause problems for usage of PSDs, but for high temperatures, PSDs as semiconductor devices suffer from a number of issues, e.g. increase of the intrinsic carrier density which reduces doping efficiency and exponential increase of junction leakage current which degrades performance and increases power consumption.^{11,12} For classical photodiode, the leakage current, also called dark current, increases shot noises, reducing signal to noise ration (SNR). Leakage current models for CMOS pixels are investigated based on a pn junction diode model and verified by simulation and measurements.¹³ As a performance index in a high temperature operation, illumination to dark ratio (IDR) is proposed to optimize the doping concentration and thickness of silicon-on-insulator photodiodes.¹⁴ Related studies on temperature influences for PSDs are

Further author information: (Send correspondence to H. W. Yoo)

H. W. Yoo: E-mail: yoo@acin.tuwien.ac.at, Telephone: +43 1 588 01 376518

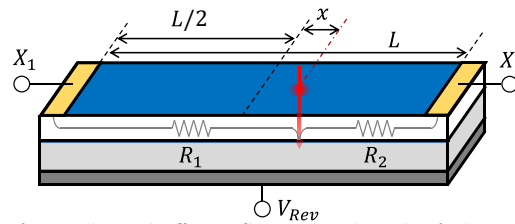


Figure 1: Schematic diagram of a 1D lateral effect PSD with a length of photo active area L . From the top, it consists of three layers of p-type resistive layer (white), high resistive intrinsic or low doped layer (bright gray), and n-type layer (dark gray) of common electrode for reverse bias voltage V_{rev} . Each end of the p-type resistive layer has electrodes X_1 and X_2 that collect divided photo current by the distances from the beam position x .

focused on the current density saturation of the diode model^{15–18} and the noise characteristics.⁶ For a thin film PSD, an enhanced operation temperature up to 120 °C is reported by suppressing saturation current density while it is indirectly verified by dark current measurements along the temperatures up to 90 °C.¹⁹ Besides the manufacturers of PSD limit the guaranteed operation temperature range to a relative small range, not allowing for operation at higher than 60 or 70 °C^{20,21} where the leakage current causes relatively small errors. So far, little attention has been paid to the temperature dependency of PSDs and the measurement performance of PSDs for elevated temperature ranges larger than 60 °C. Furthermore, compensation schemes for addressing systematic temperature-induced error reduction have not been investigated yet.

This paper investigates a degradation mechanism of position sensing accuracy for typical lateral-effect PSD in high temperature applications, and proposes a compensation scheme to eliminate or significantly reduce such device performance degradation for position sensing accuracy. In Section 2, a leakage current model of the PSD is introduced and discussed as following existing models for standard photodiodes, and a compensated scheme for the leakage current are drawn to reduce the high temperature influence in PSD measurements. Section 3 describes a PSD characterization setup for measurements of the temperature dependency of the PSD. Section 4 and 5 illustrate real world characterization measurements in terms of so-called distortion measurements and point drift measurements, in order to evaluate and prove the given leakage current model, and the proposed temperature-related position error compensation scheme. Then the conclusion is given in Section 6.

2. PSD MEASUREMENTS AT HIGH TEMPERATURES

2.1 1D lateral effect position sensitive detector

Figure 1 shows a schematic diagram of a PIN junction based lateral effect PSD with a photo active area length of L .²² From the top, the first semiconductor device layer (white) is a resistive p-type doped layer, the second layer (bright gray) is an intrinsic or low doped layer with a high resistance, and the bottom layer (dark gray) is an n-type layer for the common electrode, which is used for applying reverse bias voltage V_{rev} that improves the bandwidth of PSDs. Each end of the p-type resistive top layer has electrodes X_1 and X_2 for collecting photo currents on both sides of the PSD. When laser light shines a small spot on the active area of the PSD, photo current is generated at the local area near the beam position. The generate photo current is divided and flows into two electrodes X_1 and X_2 by the resistances R_1 and R_2 , where R_1 and R_2 are proportional to the length of travel to each electrode X_1 and X_2 , i.e. $L/2 + x$ and $L/2 - x$, respectively. By accumulating this local current division along the beam intensity distribution, the center of gravity of the beam on the PSD, simply also called as the beam position, is obtained by the measured photo current as.

$$x = \frac{L}{2} \frac{X_{RAW}}{\Sigma}, \quad (1)$$

where the raw position and the total current are defined by

$$X_{RAW} = I_{X_2} - I_{X_1}, \quad \Sigma = I_{X_1} + I_{X_2}, \quad (2)$$

and I_{X_1} and I_{X_2} denote the current from the electrodes X_1 and X_2 , respectively. Since the total current Σ represents photo current by the light in most cases, it represents the intensity information of the incident beam. At electrode of X_1 and X_2 , transimpedance amplifiers are typically used to change weak photo current to a voltage signal and the addition and the subtraction are calculated by an analog adder and subtractor.²² For the division in Eq. (1), a digital calculation is generally used to keep the precision of the measurement.

2.2 Leakage current of PSD at high temperatures

High temperature causes changes of leakage current and shunt resistance in a photodiode. In the photoconductive mode with a reverse bias voltage V_{rev} , leakage current become dominant while shunt resistor can be neglected. With the reverse bias voltage, the leakage current, also called dark current, is generated mainly by diffusion current, thermal generation, tunneling and impact ionization, which vary by the reverse bias voltage.¹³ Diffusion current is generated by the gradients of the carrier density in the quasi-neutral area, which is a part of the Shockley equation of the ideal diode law.²³ Thermal generation indicates the current by thermally induced hole-electron pairs at the depletion region.²⁴ Tunneling is a quantum-mechanical phenomenon caused by a narrow depletion region and impact ionization is due to excited hole-electron pairs caused by high energy carriers through high electric field.²³ An analysis of the classical photodiode is valid to understand behavior of PSDs at a high temperature since PSDs can be regarded as a large PIN photodiode as in Figure 1. Besides, diffusion current and thermal generation can be regarded as main leakage current sources of PSDs since tunneling and impact ionization are neglected by the PIN photodiode structure of the PSDs with a moderate reverse bias voltage.

The leakage current I_D of photodiodes can be separated into diffusion current $I_{D,diff}$ from the quasi neutral areas and the thermal generation current $I_{D,tgen}$ from the depletion area as^{13,23}

$$I_D \approx \underbrace{q \frac{n_i^2}{N_A} \sqrt{\frac{D_n}{\tau_n}}}_{I_{D,diff}} + \underbrace{q \frac{n_i}{\tau_{gen}} W}_{I_{D,tgen}}, \quad (3)$$

where

$$W = \sqrt{\frac{2\epsilon_s}{q} \left(\frac{N_A + N_D}{N_A N_D} (V_{bi} - V_{rev}) \right)}, \quad (4)$$

$$n_i \approx A \left(\frac{T}{300} \right)^{\frac{3}{2}} e^{-\frac{E_g}{2kT}}, \quad (5)$$

and q denotes the elementary charge, n_i denotes the intrinsic concentration of silicon, D_n denotes electron diffusivity, τ_n denotes the electron life time, and N_A and N_D are doping level of the p-type and n-type region, respectively. τ_{gen} is the generation lifetime, W denotes depletion width, ϵ_s denotes the dielectric constant of silicon, V_{bi} is the built-in potential in the junction, E_g is the energy bandgap of silicon, k denotes Boltzmann constant, and A is a constant defined by the density-of-state effective mass for electrons and the density-of-state effective mass of the valence band.²³ This model describes that temperature dependency of the leakage current is caused by the change of intrinsic concentration n_i along the temperature T as in Eq. (5), which is mainly defined by its exponential terms.²³ In addition, the contributions of diffusion current and the thermal generation are proportional to n_i^2 and n_i , respectively. This means that the variation of leakage current along the temperature is bounded by the variation of n_i and n_i^2 along the temperature, which can be used for verification of the leakage current model in Eq. (3) by the measurements.¹³

2.3 Compensation for high temperature influences of PSD measurements

The total current from a photodiode is a sum of the leakage current and the photo-current. Due to the symmetry of PSDs, the currents from two electrodes can be modeled as

$$I_{X_1} = I_{X_1,P} + I_{X_1,D}, \quad I_{X_2} = I_{X_2,P} + I_{X_2,D}, \quad (6)$$

where $I_{,P}$ and $I_{,D}$ are photo current and leakage current of each electrode, respectively. In contrast to the photo current, the leakage current of the PSD is not different between electrodes since a uniform or at least a symmetric structure of PSD is required in principle. Therefore position information is only found in the photo current $I_{,P}$.

In the beam position calculation of PSD in Eq. (1), this leakage current is usually neglected since it is not significant compared to photo current.¹⁸ At high temperatures, however, the influence of the leakage current is not negligible anymore. Applying Eq. (6) into Eq. (1), the conventional beam position calculation with leakage current can be rewritten as

$$x = \frac{L}{2} \frac{X_{RAW,P} + X_{D,RAW}}{\Sigma_P + \Sigma_D}, \quad (7)$$

where a raw position $X_{P,RAW}$ and the total current Σ_P by photo current and contributions of leakage currents are given as $X_{D,RAW}$ and Σ_D , i.e.

$$X_{P,RAW} = I_{X_2,P} - I_{X_1,P}, \quad \Sigma_P = I_{X_1,P} + I_{X_2,P}, \quad (8)$$

$$X_{D,RAW} = I_{X_2,D} - I_{X_1,D}, \quad \Sigma_D = I_{X_1,D} + I_{X_2,D}. \quad (9)$$

The raw position by leakage current $X_{D,RAW}$ is rather small by canceling similar leakage current of each electrodes while Σ_D increases exponentially at high temperature by Eq. (3). Therefore the beam position calculation by the conventional method in Eq. (1) leads to a reduction of the measured beam position.

To compensate for the errors by the large leakage current at high temperatures, only photo current should be counted for to retrieve the original beam position calculation. The idea of the proposed compensation scheme uses an additional measurement of the leakage current without the laser light in advance and subtract the leakage current from the measured current in Eq. (6). This lead to a compensated beam position calculation as

$$x_c = \frac{L}{2} \frac{X_{RAW} - X_{D,RAW}}{\Sigma - \Sigma_D}. \quad (10)$$

Since $X_{D,RAW}$ is rather small compared to Σ_D , the compensation results with $X_{D,RAW}$ may change minor. In practice, however, $X_{D,RAW}$ compensates for errors of asymmetric leakage current caused by manufacturing or aging of PSD. Besides, this compensation scheme is also used to reduce the influence of ambient light.²⁵

3. PSD CHARACTERIZATION SETUP

Figure 2 illustrates a schematic diagram of a PSD characterization setup. The setup has a climate chamber (KPK200,-40 to 100 °C, humidity 10 - 95 %, Feutron GmbH, Langenwetzendorf, Germany) to stress the PSD with various temperatures. In the chamber a PSD (1L30-SU2, 1D PSD, 30×4 mm active area, ceramic package with glass shielding, SiTek Electro Optics, Partille, Sweden) and its transimpedance amplifiers (AD8066, Op Amp., Analog Devices, Norwood, MA, USA) are on the two motorized translation stages (VT-80 62309110 and 62309110, 25 mm and 50 mm range, 0.5 μm resolution, ±8 μm straightness, Physik Instrumente, Karlsruhe, Germany). The laser fiber with a fiber focusing unit (CFC-5X-A, $f = 4.6$ mm, Thorlabs, Newton, NJ, USA) is fixed on the top of PSD so that the laser is focused on the PSD. The $1/e^2$ diameter of the laser spot at PSD is 106 μm. As the motorized stages move the PSD, the laser beam position on the surface of PSD changes precisely. A manual rotational mount (RP01/M, Thorlabs) is attached between the motorized stages and the PSD module for alignment of the movement directions and the PSD axis. The PSD module is mounted at the center of both stages and the rotational mount symmetrically to reduce the influence of thermal expansion in the setup. The temperature of the climate chamber is logged by a temperature sensor (176T2, PT100, Testo, Lenzkirch, Germany). Inside of the climate chamber is kept dark except the laser to eliminate influences from ambient light.

Other sensitive components to the temperature changes are outside of the climate chamber. A fiber laser diode module (OBIS 660nm LX, up to 75 mW, Coherent, Santa Clara, CA, USA) is one of the case that needs such separation to prevent the influence by temperature changes. The power of the fiber laser is adjusted by a variable fiber attenuator (VOA630-FC, Thorlabs) that ensures the class 1 operation in the lab. A DAQ card

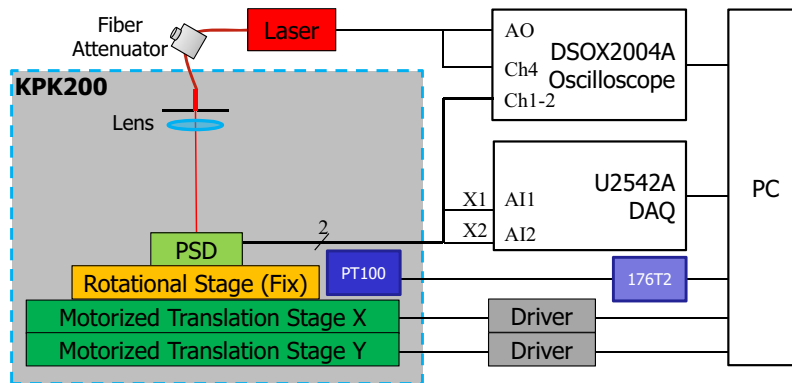


Figure 2: Schematics of the PSD characterization setup. In the climate chamber (KPK200), a 1D PSD and its readout circuit are attached on two motorized translation stages. A laser beam from the fiber is fixed and focused on the PSD while the stages laterally move the PSD. The temperature in the chamber is instantaneously logged by the PT100 probe during the experiment. A fiber laser module and a data acquisition unit are outside of the chamber in order not to be influenced by the temperature variation.

(U2542A, 500 kSps, 16 bit ADC, Keysight) records all signals from the PSD and the laser control signal, which is generated by an oscilloscope (DSOX2004A, Keysight, Santa Rosa, CA, USA). The PC controls the laser and the stages and records the beam position reading from the PSD and the temperature sensor. The setup is controlled by a Matlab script (MathWorks, Natick, MA, USA), which includes both alignment and measurement procedures.

During the experiment, the reverse voltage V_{rev} is set by 30 V, which provides a measured bandwidth of 241.8 kHz for the PSD and the transimpedance amplifiers with a gain resistor of 51.1 k Ω . L in Eq. (1) and (10) is set as 30.06 mm, obtained by the distortion measurement at 20 °C, which are explained in the following section.

4. DISTORTION MEASUREMENT OVER TEMPERATURE

Distortion measurements identify linearity of PSDs by recording beam position reading from the PSD at a number of reference beam position and by comparing the beam position measurements with the reference beam position. In the PSD characterization setup, the encoder outputs of the motorized translation stages provide the reference beam position. With temperature regulation, distortion measurements also provide more information about position sensing errors along the temperature.

The procedure of the distortion measurement consists of temperature stabilization, leakage current measurement, beam position movement, and beam position measurement. First of all the temperature in the chamber is set to the desired temperature and wait until the leakage current is stabilized. After the temperature in the climate chamber is stable, the leakage currents $I_{.D}$ of each electrode are recorded by turning off the laser. After recording the leakage current, the laser is turned on and the stages move to the desired position along a scan trajectory of the measurement area. The scan trajectory is a unidirectional raster scan, which measures full points of x and y axis in a range of 35 \times 6 mm for every 0.2 mm to check both linearity measurement along the x axis while the position dependency of the orthogonal y axis. In other words, the x axis stage moves every 0.2 mm until the end while the y axis stage is fixed. When x axis stage reaches the end, the x stage moves back to the the initial position and the y axis stage move 0.2 mm forward. The scan direction is only one-sided to avoid backlash errors. After the move of the stages, the currents from the PSD, I_{X_1} and I_{X_2} , are recorded. The signals from the PSD are recorded at 500 kSps for 0.2 second for each point. For the temperature distortion experiment, 20 °C, 40 °C, and 60 °C are chosen since the maximum operational temperature of the motorized translation stages is 60 °C for guaranteed precision and accuracy. Besides, the measurements along y axis are not discussed further since the beam position measurements do not show y position dependency.

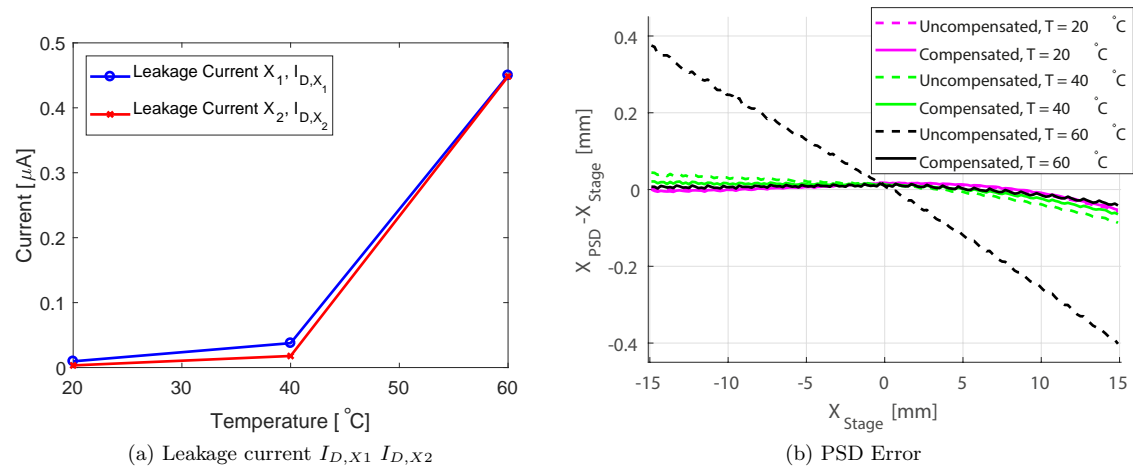


Figure 3: (left) Measured leakage current of both X_1 and X_2 during distortion measurements (right) Distortion error in uncompensated (dashed lines) and compensated case (solid lines) along temperatures of 20 °C (magenta lines), 40 °C (green lines), and 60 °C (black lines).

Table 1: RMS error of the measured distortion.

Temperature	20 °C	40 °C	60 °C
Uncompensated [mm]	0.017	0.034	0.221
Compensated [mm]	0.016	0.022	0.014

Figure 3 shows measured leakage currents and the distortion errors along the temperature. In Figure 3a, the leakage currents of both electrodes have a similar behavior for all temperature as discussed in Section 2.3. The leakage current increases up to 0.45 μA at 60 °C, which corresponds to 1.2 % of the measured photo current, which is 37.24 μA in average. The increase of the leakage current leads to a linear distortion error in position. Figure 3b illustrates that the distortion error at 60 °C with conventional beam position calculation by Eq. (1) (black dotted line) has a linear error along the beam position in x axis and 0.40 mm peak error at each end of the PSD, which corresponds to 2.7 % of the original position. The compensated beam position calculation by Eq. (10) (black solid line) can reduce this error to a value similar as in the 20 °C case. Table 1 summarizes RMS errors of the distortion measurement error for the entire PSD active area. It shows that the RMS error increases 13 times without compensation while the RMS errors with the compensation scheme stay low.

5. POINT DRIFT MEASUREMENT

From the distortion measurement, it is proved that increased leakage currents at high temperature are the main source of the PSD distortion and this distortion is only linear along the distance as discussed in Section 2.3. For temperatures higher than 60 °C, however, distortion measurement is not possible because of the operation temperature limit of the motorized stages. Most applications in automotive industries, for example, require high temperatures at least over 85 °C for electronics test.¹⁰ To use PSDs in such harsh environment tests, the compensated beam position calculation by Eq. (10) has to be also evaluated for high temperatures above 60 °C. Point drift measurement excludes the problematic stages from the measurements by fixing the laser at a point and measures the drift of the beam position reading as the temperature changes. By turning off the motorized stages, the temperature can be extended up to 95 °C. By point drift measurement, the model of the leakage currents as well as the compensated beam position calculation can be verified for a wider temperature range.

The procedure of the point drift measurements is as follows. First, the stages move the PSD to a desired position and then are plugged off from the power supply. After the position of the beam and PSD is fixed, the

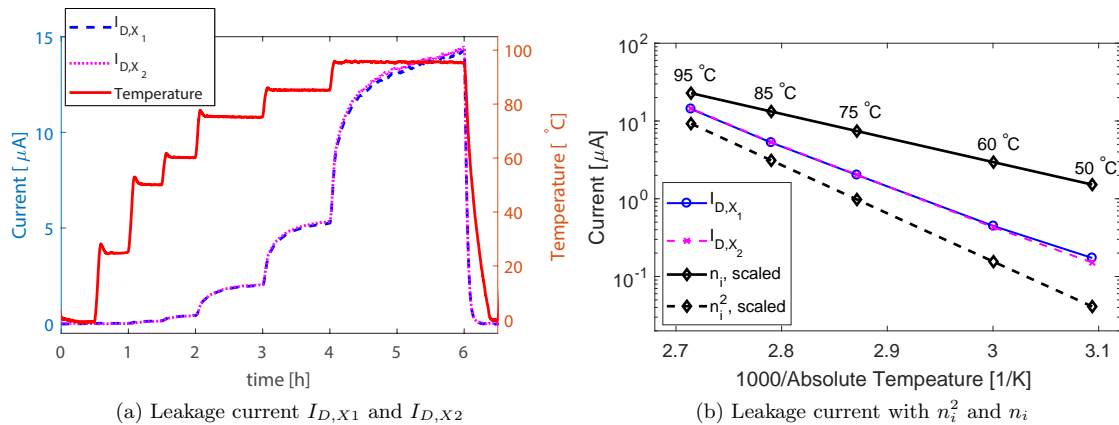


Figure 4: (left) Measured leakage current along various temperature from 0 to 95 °C (right) its redrawn diagram in a log scale versus $1000/T$ with the diffusion current the and thermal generation model in Eq (3).

climate chamber runs by a given temperature profile while the temperature sensor records the temperature in the climate chamber for every second. While the temperature varies by time, a pair of both leakage current of $I_{X1,D}$ and $I_{X2,D}$ and the current of I_{X1} and I_{X2} are recorded for every 6 seconds. In the measurements, the position of the beam is chosen as 13 mm, measured at 25 °C, which is enough distance from the center of the active area but not an edge of the PSD.

5.1 Leakage current measurements

Figure 4a illustrates the transient responses of the leakage current along the temperature profile from 0 °C to 95 °C. The temperature of the climate chamber is set as 0 °C, 25 °C, 50 °C, 60 °C, 75 °C, 85 °C, and 95 °C with a duration of 30 minutes up to 50 °C, 1 hour up to 85 °C, and 2 hours at 95 °C. The leakage currents of both electrodes are almost identical at high temperatures. A slow transient response of the leakage current is observed, which can be due to the heat transfer from the hot air in the climate chamber to the PSD chip through the ceramic package with a glass cover, but the cause is not clarified in this paper.

Figure 4b describes the variation of the measured leakage currents of each electrode along the axis of $1000/K$.^{13,23} n_i^2 and n_i of Si are drawn to compare the gradient of the diffusion current and the thermal generation with the measured leakage current, respectively, but are arbitrarily scaled since the absolute parameters of layers are unknown. The gradients of the leakage current show a good agreement with the model in Eq. (3), which is a compromised gradient value of 5.40 between n_i of 3.09 and n_i^2 of 6.18 in Figure 4b.¹³ This result means that the mechanism of the leakage current of the PSD follows the leakage current model of the silicon photodiode in Section 2.2.

5.2 Point drift measurement

Figure 5 illustrates the measured beam position and total current by the point drift measurement in Figure 4. The conventional beam position calculation in Eq. (1) leads to the measured beam position from 13.00 mm down to 7.19 mm (blue dashed line in Figure 5a and 5b). By the compensated beam position calculation in Eq. (10), the beam position sensing error is suppressed in $\pm 20 \mu\text{m}$ peak to peak except for a drastic changes of temperature from 95 °C to 0 °C (black solid line in Figure 5a and 5b). This corresponds to a reduction of the beam position sensing error from 44.7 % to 0.2 %. The source of the error is shown in the total current Σ and Σ_c in Figure 5c and 5d. The uncompensated total current increases from 37 μA to 65 μA while the compensated case shows only a μA range of fluctuation. This shows that the proposed compensated beam position calculation can significantly improve the beam position measurement error of PSDs, enabling usage of PSDs in high temperature applications such as reliability tests for automotive applications.

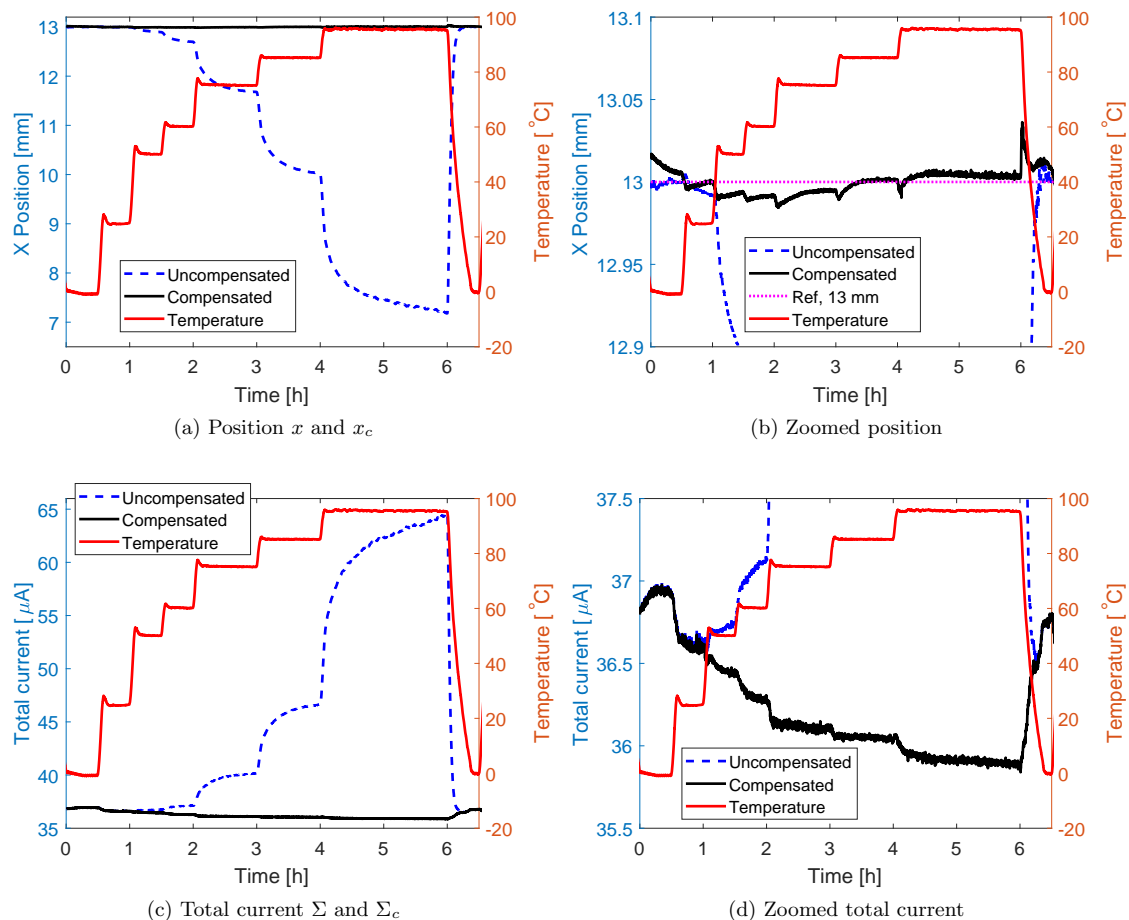


Figure 5: Point drift measurements of 1D PSD with various temperature from 0 to 95 °C. The measured beam position (top figures) is shown with conventional beam position calculation x (blue dashed line) and the compensated beam position calculation x_c (black solid line). The total current Σ and Σ_c (bottom figures) shows a similar manner as the position calculation.

6. CONCLUSION

This paper investigates temperature dependency of lateral effect 1D PSDs based on the classical leakage current model of standard photodiodes, and proposes a novel compensation method to eliminate temperature-induced position sensing errors in PSDs at elevated temperatures up to 95 °C. At high temperatures, leakage current of the PSD increases by the diffusion current and thermal generation, leading to a systematic error of the measured beam position significantly. To compensate for this systematic error at high temperatures, a compensation scheme is proposed, which utilizes additional reading of the PSD while the light source is turned off. To verify the proposed leakage model and compensation scheme, a PSD characterization setup is developed with two motorized translation stages and a 1D PSD module in a climate chamber and an isolated fiber laser source and a data acquisition system at outside of the chamber. Distortion measurements use two motorized stage to compare the beam position reading of the PSD with the actual beam position by the stage encoders. The distortion measurement results show up to 2.7 % position sensing error at 60 °C while the compensation scheme reduces this to the error level of 20 °C. For the evaluation at higher temperatures, a special point drift measurement is

proposed. This measurement uses a fixed beam point on PSD and records the leakage current and beam position reading during the temperature change from 0 °C up to 95 °C. For the beam spot at 13 mm measured at 25 °C, the measured beam position varies down to 7.19 mm at 95 °C, corresponding to a relative position error of 44.7 %. By applying the proposed compensation method, this error is reduced to 0.2 %, meaning a remaining systematic deviation of 20 μm . Again, the compensation scheme nearly eliminates the temperature-induced position sensing errors of the PSD at least until 95 °C.

The proposed compensation method enables usage of 1D lateral PSDs up to high temperatures of 95 °C, with unchanged position sensing accuracy. This extends the usable application scenarios for PSDs, and provides e.g. now a possibility for micro scanner characterizations at elevated temperatures. Besides, the results on the leakage current model and the compensated scheme can be extended to 2D lateral effect PSDs and segmented PSDs as well since the principle is similar. The slow transient of the measured leakage current of the PSD is also necessary to be investigated as a potential source of the errors in compensation. The noise analysis of the compensated scheme can be also considered. Not only the software and system improvement, a device-level design of PSDs for low leakage currents as Ref. 19 and Ref. 26 can be also interesting for further extending the usage of PSDs in various high temperature applications.

ACKNOWLEDGMENTS

This work has been supported in part by the Austrian Research Promotion Agency (FFG) under the scope of the LiDcAR project (FFG project number 860819).

REFERENCES

- [1] Wallmark, J. T., "A New Semiconductor Photocell Using Lateral Photoeffect," *Proceedings of the IRE* **45**(4), 474–483 (1957).
- [2] Neal, D. R., Copland, J., and Neal, D. A., "Shack-Hartmann wavefront sensor precision and accuracy," in [*Advanced Characterization Techniques for Optical, Semiconductor, and Data Storage Components*], **4779**, 148–161, International Society for Optics and Photonics (2002).
- [3] MacLachlan, R. A. and Riviere, C. N., "High-Speed Microscale Optical Tracking Using Digital Frequency-Domain Multiplexing," *IEEE Transactions on Instrumentation and Measurement* **58**(6), 1991–2001 (2009).
- [4] Francini, F., Macchiarulo, M., Tiribilli, B., and Buah-Bassuah, P. K., "Opto-electronic system for displacement and vibration measurements," *Review of Scientific Instruments* **58**(9), 1678–1681 (1987).
- [5] Meyer, G. and Amer, N. M., "Novel optical approach to atomic force microscopy," *Applied Physics Letters* **53**(12), 1045–1047 (1988).
- [6] Makynen, A., Kostamovaara, J. T., and Myllyla, R. A., "Displacement sensing resolution of position-sensitive detectors in atmospheric turbulence using retroreflected beam," *IEEE Transactions on Instrumentation and Measurement* **46**(5), 1133–1136 (1997).
- [7] Andersson, H. A., Manuilskiy, A., Thungström, G., and Nilsson, H.-E., "Evaluation of an integrated Fourier-transform spectrometer utilizing a lateral effect position sensitive detector with a multi-channel Fabry-Perot interferometer," *Measurement Science and Technology* **19**(4), 045306 (2008).
- [8] Hofmann, U., Janes, J., and Quenzer, H.-J., "High-Q MEMS Resonators for Laser Beam Scanning Displays," *Micromachines* **3**(2), 509–528 (2012).
- [9] Yoo, H. W., Druml, N., Brunner, D. and Schwarzl, C., Thurner, T., Hennecke, M., and Schitter, G., "MEMS-based lidar for autonomous driving," *Elektrotechnik und Informationstechnik* **135**(6), 408–418 (2018).
- [10] Volkswagen, *Electric and Electronic Components in Motor Vehicles up to 3.5 t: General Requirements, Test Conditions and Tests* (2013). Ver. 2.2.
- [11] Dreike, P. L., Fleetwood, D. M., King, D. B., Sprauer, D. C., and Zipperian, T. E., "An overview of high-temperature electronic device technologies and potential applications," *IEEE Transactions on Components, Packaging, and Manufacturing Technology: Part A* **17**(4), 594–609 (1994).
- [12] Watson, J. and Castro, G., "A review of high-temperature electronics technology and applications," *Journal of Materials Science: Materials in Electronics* **26**(12), 9226–9235 (2015).

- [13] Loukianova, N. V., Folkerts, H. O., Maas, J. P. V., Verbugt, D. W. E., Mierop, A. J., Hoekstra, W., Roks, E., and Theuwissen, A. J. P., "Leakage current modeling of test structures for characterization of dark current in cmos image sensors," *IEEE Trans. on Electron Devices* **50**, 77–83 (2003).
- [14] Novo, C., Giacomini, R., Doria, R., Afzalian, A., and Flandre, D., "Illuminated to dark ratio improvement in lateral SOI PIN photodiodes at high temperatures," *Semiconductor Science and Technology* **29**(7), 075008 (2014).
- [15] Woltring, H. J., "Single- and dual-axis lateral photodetectors of rectangular shape," *IEEE Trans. on Electron Devices* **22**, 581 – 590 (1975).
- [16] Connors, W. P., "Lateral photodetector operating in the fully reverse-biased mode," *IEEE Transactions on Electron Devices* **18**(8), 591–596 (1971).
- [17] Noorlag, D. J. W. and Middelhoek, S., "Two-dimensional position-sensitive photodetector with high linearity made with standard i.c.-technology," *IEE Journal on Solid-State and Electron Devices* **3**(3), 75–82 (1979).
- [18] Qian, D., Wang, W., and Busch-Vishniac, I. J., "A method for measurement of multiple light spot positions on one position-sensitive detector (PSD)," *IEEE Transactions on Instrumentation and Measurement* **42**(1), 14–18 (1993).
- [19] Fortunato, E., Lavareda, G., Martins, R., Soares, F., and Fernandes, L., "Large-area 1D thin-film position-sensitive detector with high detection resolution," *Sensors and Actuators A: Physical* **51**(2), 135–142 (1995).
- [20] Hamamatsu, *Two-dimensional PSD: S5990-01, S5991-01, Improved tetra-lateral type for surface mounting* (2013).
- [21] SiTek, *Datasheet of 1L30 SU2: 30 mm 1D PSD High Linearity Position Sensing Detector* (2005).
- [22] Hamamatsu, *Opto-semiconductor handbook, Chap.2 Si Photodiodes* (2014).
- [23] Sze, S. and K. Ng, K., [*Physics of Semiconductor Devices*], John Wiley & Sons, Inc., 3 ed. (2007).
- [24] Khanna, V. K., "Carrier lifetimes and recombination-generation mechanisms in semiconductor device physics," *European Journal of Physics* **25**(2), 221–237 (2004).
- [25] Zhou, C., Wang, W., Chao, H., Hong, L., Cao, X., Zhang, P., and Chu, L., "The study on the method of eliminating errors of psd," *Sensors and Transducers* **25**, 52–57 (2013).
- [26] Kim, H. J., Cho, G., Choi, J., and Jung, K.-W., "Leakage current of amorphous silicon p-i-n diodes made by ion shower doping," *Applied Physics Letters* **80**(25), 4843–4845 (2002).